SPST Acoustic Switch Based on Poled Ferroelectrics

Hersh Desai, Milad Zolfagharloo Koohi, Amir Mortazawi
Department of Electrical Engineering and Computer Science, University of Michigan, USA
{herdes, milad, amirm}@umich.edu

***Abstract*—The first proof-of-principle demonstration for a single-pole single-throw (SPST) acoustic switch using phase inversion in ferroelectric bulk acoustic wave (BAW) resonators is presented. Independent control of piezoelectric coefficient in two shunt ferroelectric acoustic resonators is leveraged to implement the switch. The operating principle of the switch can be extended to any ferroelectric acoustic structure. Furthermore, the switch technology presented herein is suitable for replacing transistor-based switches for channel selection in acoustic filter banks for radio frequency front ends (RFFE). A prototype is presented utilizing stacked crystal filters (SCF) made from Barium Strontium Titanate (BST) providing isolation of 41.4 dB in the OFF state and insertion loss of less than 3.7 dB in the ON state. The switch prototype's operating frequency is 3.6 GHz. The total active area of the resonators is 1126 μm².**

***Keywords*— radio frequency (RF) switch, microwave filters, bulk acoustic wave (BAW) devices, barium strontium titanate (BST), ferroelectric films**

I. Introduction

Wireless communication has reached a level of sophistication that necessitates new technologies that both improve performance and reduce complexity. Microwave filters are a key component in the analog-mixed signal chain required for wireless transceivers. Micro-electrical-mechanical systems (MEMS) acoustic resonators are a leading technology in microwave filters for mobile wireless communications. Among available technologies, BAW devices offer low power consumption, compact device size, low insertion loss, and steep filter skirts [1,2]. However, RFFE's often require many filters organized into large filter banks to cover the spectrum necessitating an extensive network of solid-state switches. This switch matrix adds to system overhead in terms of power consumption, space, and integration complexity [3]. Transistor-based switches are fast, reliable, and reasonably sized, but do not share a fabrication process with acoustic filter technologies. Integrating acoustic filters with switches is one effective pathway for reducing RFFE complexity. This work presents a proof-of-concept channel selection solution with extremely low power consumption, small footprint, low insertion loss, high isolation, and compatibility with BAW fabrication processes as shown in Fig. 1.

This work presents a prototype acoustic switch that leverages poling dependent phase shifting in BAW resonators. Furthermore, the switch is highly amenable to integration with other microwave acoustic devices such as filters. Additionally, this work verifies the operating principle of the prototype through supporting measurements. The device uses two resonators in parallel that can selectively prove a 180-degree phase shift. The resonators are fabricated on a silicon substrate. The prototype has insertion loss of 3.7 dB when ON and isolation of over 41.4 dB in OFF state. The active area of the device is 1126 μm². The following sections include simulation, theoretical discussion, and experimental verification.

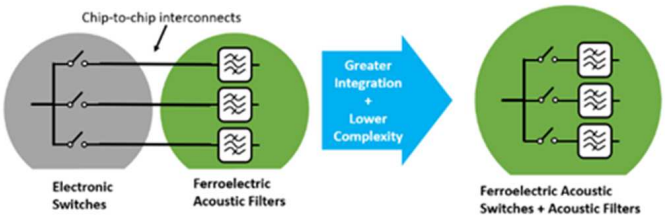

Fig. 1. Motivation for ferroelectric switches to replace electronic switches.

II. Principle of Operation

Ferroelectric materials are a subclass of piezoelectric materials with the property of having spontaneous polarization that can be oriented with the application of an external electric field. The presence of an electric dipole within the crystalline unit cell allows for transduction between acoustic and electrical energy. The orientation of the dipoles (the overall polarization vector direction) affects the magnitude and sign of the coefficients in the piezoelectric tensor. The piezoelectric tensor relates strain and electric field in the strain-charge form [4]:

$$S = sT + dE, \quad (1)$$

$$D = dT + eE. \quad (2)$$

In this work, the piezoelectric coefficient d_{33} of a bilayer ferroelectric BAW device is controlled to provide two states of phase delay, 180 degrees apart. The ferroelectric material chosen for this work is BST because it exhibits paraelectric behaviour at room temperature removing the need for complicated poling procedures to direct the polarization vector. However, the switch operation is agnostic to the choice of ferroelectric material.

A typical crystalline structure in ferroelectrics is the centrosymmetric cubic perovskite unit cell. Applied electric field is capable of breaking inversion symmetry in the unit cell and inducing piezoelectricity. When a constant electric field, E_{dc}, is applied, a small signal electric field experiences an effective piezoelectric coefficient d_{eff}. The effective small signal piezoelectric coefficient d_{eff} in the film is [5]

$$\frac{ds}{dE}|_{E_{DC}} = d_{eff} = 2\alpha\chi^2 E_{DC}, \quad (3)$$

where α is the electromechanical coupling coefficient and χ is the susceptibility. Notably, a negative effective piezoelectric coefficient is achievable for small signal excitations under negative E_{dc}.

The structure of switch consists of two stacked crystal filters (SCF) because the electrical path between input and output ports is severed due to shielding provided by the grounded middle electrode [6]. As depicted with two poling

2024 IEEE/MTT-S International Microwave Symposium - IMS 2024 | 979-8-3503-7504-6/24/$31.00 ©2024 IEEE | DOI: 10.1109/IMS40175.2024.10600205

configurations in Fig. 2a and Fig. 2b, the SCF is composed of two transducer layers vertically stacked. By switching between the two poling configurations, phase of signal transferred through the SCF can be inverted. RF present at the input of the device is converted to an elastic vibration. The strain carried by that wave will produce a voltage on the other electrode through the inverse piezoelectric effect. Inverting the polarization state of either the input or output transducer shifts the transmitted signal by 180 degrees, as shown in Fig. 2d.

The equivalent circuit model for a single SCF presented in Fig. 2c expands upon the mBVD model for an acoustic resonator. Each layer of BST has an electrical branch (C_e and R_e) in parallel with a motional branch (R_m, L_m, and C_m). The motional branches for each layer are coupled by a transformer with a turn ratio of 1:1. The polarization state is modelled as the orientation and turn ratio of the transformer. There is a parasitic stray capacitance between the input and the output ports, represented by C_p with a dashed line. The effective electromechanical coupling coefficient, K_t^2, and anti-resonance frequency, f_a, can be set according to the acoustic transmission line model, which then can be used to calculate the lumped components of the model by (4) - (7).

$$f_r = \frac{f_a}{2}\left(1 + \sqrt{1 - \frac{16K_t^2}{\pi^2}}\right) \quad (4)$$

$$C_m = C_e\left[\left(\frac{f_a}{2}\right)^2 - 1\right] \quad (5)$$

$$L_m = \frac{1}{C_m(2\pi f_r)^2} \quad (6)$$

$$R_m = \frac{2\pi f_r L_m}{Q_m} \quad (7)$$

Finally, through full-wave simulation of the total structure in HFSS, the expected value of the stray capacitance between the ports, C_p, is also obtained.

The acoustic switch operates by splitting energy into two pathways and recombining it either in phase or out of phase leading to either coherent or destructive interference. The device is realized by connecting two SCFs parallel with independent control of polarization (independent voltage sources). The switch is turned ON by poling both SCF's in the same state allowing energy to meet in phase and combine coherently. Conversely, the switch is turned OFF by reversing the poling in either SCF creating a 180-degree delay in that device and causing destructive interference at the output. Each polarization state is associated with the switch being either ON or OFF. The acoustic switch is illustrated with poling configurations for both ON and OFF states as well as simulated S-parameters ignoring material and conductor losses. Lossless simulation is shown to highlight the nature of the phenomenon.

III. Fabrication Process

The fabrication process flow for the resonator structure is depicted in Fig. 4. The switch is fabricated on high resistivity silicon substrate. The process starts by thermal oxidation of silicon. After that, the platinum bottom electrodes are deposited and patterned by evaporation and lift-off. Next, the first ferroelectric BST transduction layer is sputter deposited at 650 °C in a 45 mTorr Ar and O_2 environment (with a 4 to 1 partial pressure ratio). The ferroelectric BST thin film here has a

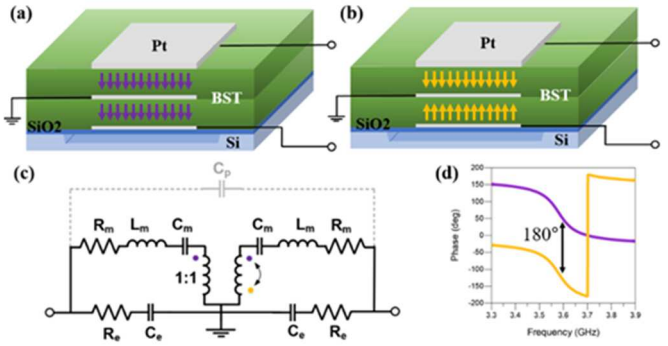

Fig. 2. Illustration of SCF with (a) layers poled the same direction and (b) layers poled in opposite directions. (c) Equivalent circuit model for a single SCF. The purple and yellow dots correspond to the polarization states shown in (a) and (b). (d) Simulated phase of transmitted signal through single SCF under polarization states depicted in (a) and (b).

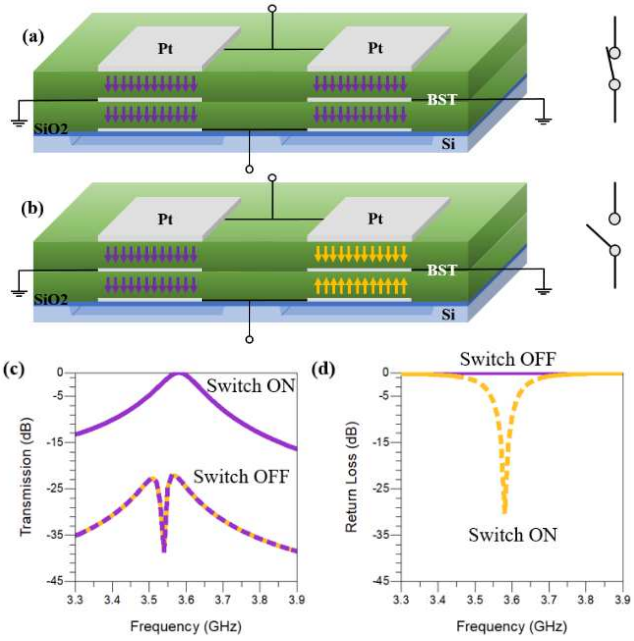

Fig. 3. Illustration and simulation of acoustic switch. (a) ON state switch with both SCF's poled in the same configuration. (b) OFF state switch with SCF's poled in differing configuration. (c) Simulated insertion loss and isolation of switch in both ON and OFF states respectively. (d) Return loss of switch in both ON and OFF states.

composition ratio of x = 0.5, which corresponds to a Curie temperature of -20°C and paraelectric phase at room temperature. Next, the platinum middle electrode and the second BST layer are deposited by evaporation and sputtering respectively by a similar process to the first set of layers. The platinum middle electrodes are patterned before the second layer of BST is sputtered. Platinum top electrode is deposited by evaporation and patterned by lift-off. Afterward, the BST films and silicon dioxide layer are wet etched in buffered hydrofluoric acid (BHF) to form the release windows and the vias to the middle and bottom electrodes. A 1.5 µm aluminum/gold layer is deposited by evaporation and patterned by lift-off to create contacts for probing the devices. Finally, the silicon substrate beneath the devices' active area is undercut in a 3 Torr xenon difluoride environment to release the devices.

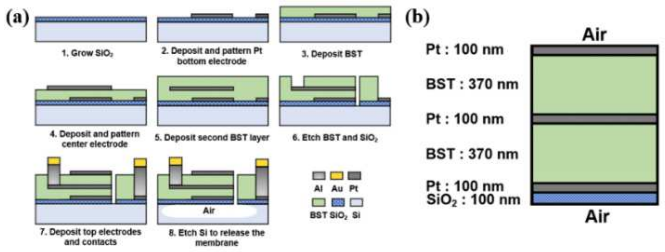

Fig. 4. (a) Fabrication process flow for ferroelectric SCF. BST is deposited by RF magnetron sputtering. All electrodes are platinum. Contacts are aluminum coated with gold. (b) Layer thicknesses chosen for BST resonator.

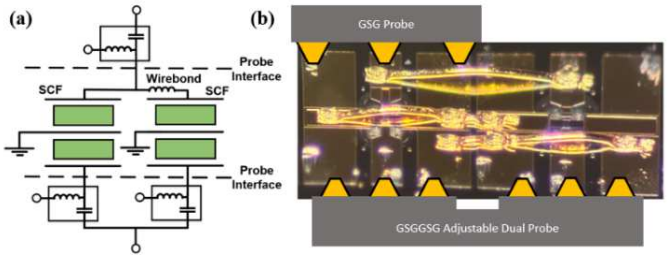

Fig. 5. (a) Illustration of measurement set-up and (b) microphotograph of acoustic switch with test fixtures. Dashed probe interface lines in (a) correspond to the illustrated RF probes in (b).

The device layer stack-up in the active region of the resonators is presented in Fig 4b. The dimensions presented were determined using an acoustic transmission line model. Platinum electrode thickness was set to 100 nm and the thickness of BST and silicon dioxide were optimized to set the resonant frequency and maximize electromechanical coupling coefficient.

Fig. 5a depicts two resonators bonded together to realize the acoustic switch, and Fig. 5b presents the fabricated and measured device. The wire bond is treated as a series lumped inductor in the simulations provided in Fig. 3c and Fig. 3d. Although the grounds are connected through middle electrode within the SCF's, they also have been bonded together. S-parameter measurement of an acoustic switch was conducted using a wafer probe station and an Agilent E8364C Vector Network Analyzer.

IV. Results

The switch S-parameter measurement is presented to demonstrate insertion loss, isolation, and bandwidth. Measurements were performed on a vector network analyzer with 50 Ohm reference impedance. Short-open-load-through (SOLT) calibrations were performed at the probe tips using a wafer calibration impedance standard substrate. Mismatches at the device ports were handled using lumped element matching networks in Advanced Design System.

Transmission (insertion loss and isolation) measurements for the acoustic switch were measured in the ON and OFF states and are presented in Fig. 6a. In the ON state, insertion loss of 3.7 dB is observed and in the OFF state, peak isolation of 41.4 dB is observed. The 3dB fractional bandwidth of the ON state response is 4.4%. The return loss of the switch is presented in Fig. 6b in both ON and OFF states.

A fully integrated version of this prototype is under

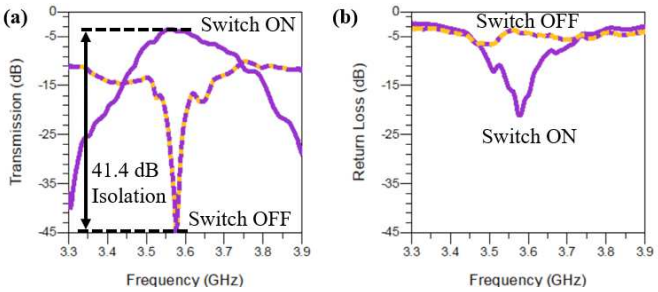

Fig. 6. S-parameter measurement of acoustic switch. (a) Measured insertion loss (ON state) and isolation (OFF state) of acoustic switch. (b) Measured return loss of the switch in both ON and OFF states.

development. In addition, experimental work is ongoing to characterize the linearity and switching speed of this switch technology. Previous work has shown experimentally, that the switching speed of BST acoustic resonators is less than 100 ns [7], comparable to electronic RF SPST switches found on the market. Furthermore, the resonator performance did not degrade after 109 switching cycles. Regarding linearity, the IIP3 of BST thickness mode resonators operating around 2 GHz was found to be 39 dBm [8].

V. Conclusion

To the best knowledge of the authors, this work marks the first demonstration of an acoustic switch based on phase inversion in ferroelectric acoustic resonators. The prototype switch is fabricated from RF magnetron sputtered BST SCFs on Si wafer. For this first demonstration, two individual resonators were wire-bonded together, but this switch can be realized in a fully integrated implementation. The fabricated switch prototype has insertion loss of 3.7 dB, isolation of 41.5 dB, and 3dB fractional bandwidth of 4.4%. The acoustic switch presented here represents an alternative to transistor switches for RFFE's and shares a fabrication process with high-performance BAW microwave filters.

Acknowledgment

The fabrication was performed at the Lurie Nanofabrication Facility at the University of Michigan.

References

[1] Yang, Kai, Chenggong He, Jiming Fang, Xinhui Cui, Haiding Sun, Yansong Yang, and Chengjie Zuo. "Advanced RF filters for wireless communications." *Chip* (2023): 100058.

[2] C. C. W. Ruppel, "Acoustic Wave Filter Technology–A Review," in *IEEE Transactions on Ultrasonics, Ferroelectrics, and Frequency Control*, vol. 64, no. 9, pp. 1390-1400, Sept. 2017.

[3] R. Ruby, "A Snapshot in Time: The Future in Filters for Cell Phones," in *IEEE Microwave Magazine* , vol. 16, no. 7, pp. 46-59, Aug. 2015.

[4] Ikeda, Takurō. *Fundamentals of piezoelectricity*. Oxford university press, 1996.

[5] M. Z. Koohi. "Reconfigurable Bulk Acoustic Wave Resonators and Filters Employing Electric-field-induced Piezoelectricity and Negative Piezoelectricity for 5G." PhD diss., University of Michigan, Ann Arbor, 2020.

[6] M. Z. Koohi, S. Nam and A. Mortazawi, "Intrinsically Switchable Miniature Ferroelectric Stacked Crystal Filters," *2019 IEEE MTT-S International Microwave Symposium (IMS)*, Boston, MA, USA, 2019, pp. 661-664, doi: 10.1109/MWSYM.2019.8700965.

[7] V. Lee, S. Lee, S. A. Sis and A. Mortazawi, "Switching reliability and switching speed of barium strontium titanate (BST) BAW devices," in

2014 44th European Microwave Conference, Rome, Italy, 2014, pp. 500-503

[8] M. Z. Koohi and A. Mortazawi, "On the Linearity of BST Thin Film Bulk Acoustic Resonators," *2018 IEEE MTT-S International Microwave Workshop Series on Advanced Materials and Processes for RF and THz Applications (IMWS-AMP),* Ann Arbor, MI, USA, 2018, pp. 1-3.